ORIGINAL RESEARCH

Characterization of Optimized TiO₂ Nanotubes Morphology for Medical Implants: Biological Activity and Corrosion Resistance

Ricardo Pereira Nogueira[1,2]
Jose Deuzimar Uchoa[3,4]
Fanny Hilario[2]
Gabriela de Fátima Santana-Melo [5]
Luana Marotta Reis de Vasconcellos [5]
Fernanda Roberta Marciano [6]
Virginie Roche[2]
Alberto Moreira Jorge Junior [2,7]
Anderson Oliveira Lobo [4]

[1]Chemical Engineering Department, Khalifa University of Science and Technology, Abu Dhabi 127788, United Arab Emirates; [2]Université Grenoble Alpes, Université Savoie Mont Blanc, CNRS, GrenobleINP*LEPMI, Grenoble 38000, France; [3]Federal Institute of Education, Science and Technology of Piauí, Teresina 64053-390, Brazil; [4]Interdisciplinary Laboratory for Advanced Materials, BioMatLab Group, Materials Science and Engineering Graduate Program, UFPI – Federal University of Piaui, Teresina 64049-550 Brazil; [5]Department of Bioscience and Oral Diagnosis, Institute of Science and Technology, Sao Paulo State University, Sao José dos Campos 12245-000, Brazil; [6]Department of Physics, Federal University of Piaui, Teresina PI 64049-550 Brazil; [7]Department of Materials Engineering, Federal University of São Carlos, São Carlos 13565-905, Brazil

Correspondence: Anderson Oliveira Lobo
Campus Universitário Ministro Petrônio Portella, Av. Universitária, s/n, Centro de Tecnologia, Laboratório Interdisciplinar de Materiais Avançados, Ininga, Teresina, PI 64049-550, Brazil
Tel +55 86 32371057
Email lobo@ufpi.edu.br

Background: Nanostructured surface modifications of Ti-based biomaterials are moving up from a highly-promising to a successfully-implemented approach to developing safe and reliable implants.

Methods: The study's main objective is to help consolidate the knowledge and identify the more suitable experimental strategies related to TiO₂ nanotubes-modified surfaces. In this sense, it proposes the thorough investigation of two optimized nanotubes morphologies in terms of their biological activity (cell cytotoxicity, alkaline phosphatase activity, alizarin red mineralization test, and cellular adhesion) and their electrochemical behavior in simulated body fluid (SBF) electrolyte. Layers of small-short and large-long nanotubes were prepared and investigated in their amorphous and crystallized states and compared to non-anodized samples.

Results: Results show that much more than the surface area development associated with the nanotubes' growth; it is the heat treatment-induced change from amorphous to crystalline anatase-rutile structures that ensure enhanced biological activity coupled to high corrosion resistance.

Conclusion: Compared to both non-anodized and amorphous nanotubes layers, the crystallized nano-structures' outstanding bioactivity was related to the remarkable increase in their hydrophilic behavior, while the enhanced electrochemical stability was ascribed to the thickening of the dense rutile barrier layer at the Ti surface beneath the nanotubes.

Keywords: surface modification, TiO₂ nanotubes, commercially pure titanium, bioactivity

Introduction

Thanks to a remarkable combination of mechanical and physicochemical properties, Titanium (Ti) is broadly used in a large panel of biomedical implants, from dental screws through femoral components to total hip replacement.[1] Admittedly, Ti combines low density (~4.5 g/cm³) and high tensile strength (275–412 MPa) with, which is of uttermost importance, a lower elastic modulus (~100 GPa) compared to other metallic implant materials like 316L stainless steel (~200 GPa) and CoCrMo alloys (~240 GPa). Therefore, the Ti elastic modulus is much closer to the bones' one (ca 10–30 GPa),[1,2] thus considerably limiting stress shielding effects—the transfer of the physiological loading from the bone to the stiffer implant with the consequent risk of osteopenia (reduction in bone density). Beyond these mechanical aspects, Ti is notably biocompatible,[3] promoting cell growth and differentiation.[4–6]

Metallic biomedical implants must also have outstanding corrosion resistance to the different aggressive body fluids to ensure the long-term necessary mechanical performance and avoid undesired or toxic ions release. Ti undeniably meets those requirements due to its highly passivating behavior, i.e., its ability to develop—almost instantaneously—a continuous, uniform, and high-protective TiO_2 nanometric-thick film upon the surface.[1,2,7] Nevertheless, this high protectiveness also means high physicochemical stability that hampers interfacial interactions so that, in its native form, the passive film tends to be bioinert.[8] A highly promising approach to overcome this potential drawback is to modify the implants' surface to increase bioactivity (bone-bonding ability).

One way to improve bone-bonding ability is to grow self-assembled TiO_2 nanotubes (NTs) upon the Ti surface through anodization,[9] followed by different heat treatments. The typical anodization protocol for the development of TiO_2 nanotubes consists of applying a well-controlled potential difference (a few tens of volts) across the metal | electrolyte interface between the metallic Ti and a fluoride-rich electrolyte. This potential difference acts as the driving force for the further oxidation of the previously passivated Ti surface. The growth of the highly organized self-assembled nanotube layer is the result of the complex interplay between the overall oxide layer thickening and the counteracting effects of local dissolution triggered by the fluoride anions as well as internal mechanical stresses inside the oxide layer. The tubes' morphology (length, diameter, spacing, wall thickness) can be tuned by adjusting the applied potential, anodization time, electrolyte nature (aqueous or organic), temperature, fluoride ions concentration, and pH.[10–13] In most experimental conditions, TiO_2 nanotubes grow amorphous but can be crystallized afterward by heat treatment either into anatase or, at higher temperatures, a mix of anatase and rutile phases.[10,14–18]

Those different tunable features of the nanotube layer—morphology, topography, crystalline structure—open up the way to a large panel of surface properties leading, for instance, to controlled surface contact angles and wettability. These different properties strongly affect bioactive and biological responses, so that knowing how they depend on the nanotubes' characteristics is crucial for the enhancement of implant material surfaces. Indeed, compared to the smooth titanium surface, nanotube-modified surfaces are much more bioactive, accelerating the rate of apatite formation and improving bone cell adhesion and proliferation.[14,19] Additionally, the nanotubular structure's high specific surface area improves tissues' contact, favoring bone tissues' growth and enhancing the bonding strength between the implant material and human bones.[20]

The literature about TiO_2 nanotubes is vast and broad, involving several aspects of their structure, morphology, and properties. However, its exhaustive survey is far beyond the objective of the present paper, in which we propose a set of references that are deemed to ensure the self-readability of the manuscript and the necessary complementary information. One of the approaches that deserve to be investigated more systematically concerns the biological—corrosion responses, in which experimental results are discussed as a function of the morphology of the nanotubes and their structure, amorphous or crystalline.

In this sense, in a recent work, Hilario et al[21] have studied the influence of morphology and crystalline structure of TiO_2 nanotubes on electrochemical properties and bioactivity. Results showed that anodized titanium has considerably better corrosion resistance and bioactivity than smooth Ti substrates. The as-anodized amorphous nanotubes were annealed and modified into different crystalline structures more suitable for biomedical applications. Specifically, the study highlighted that a combined anatase-rutile structure was preferable because of the synergy brought by better chemical stability and mechanical properties than a simple anatase structure, despite the latter's better bioactivity.

The nanotube-modified topography, surface energy, and chemistry are other essential features as they can significantly change the biological activity of cells cultivated *in vitro* on titanium as well as the *in vivo* bone-implant bonding properties.[22–24] Other studies pointed out the beneficial effects of the nanotube layer on *in vitro* osteogenesis and *in vivo* osteointegration[25–27] due to both modified surface chemistry and nanostructured topography.[23] Also interesting, specific topographies coupled to specific proteins may impact growth factors and enhance cell adhesion, viability, and differentiation at the early stages of bone regeneration.[28] Indeed, Jie et al[29] have reported that the nanoscale topography of anatase phase titania film affects surface contact angles and wettability, leading osteoblasts to spread and grow swiftly with enhanced adhesion, proliferation, and differentiation.

As mentioned before, to the best of our knowledge, little attention has been devoted to the straightforward

correlation between the physicochemical and topological characteristics of the nanotube layers and the coupled corrosion-bioactivity behavior. This study thus aimed to assess the pertinence of TiO_2 nanotubes as a surface modification technique for implant devices by taking into account both the biological and corrosion-resistance aspects. Based on a previous study,[21] two optimized nanotubes morphologies were held to be investigated. While in that previous paper, the biological approach was only introductory and restricted to the apatite formation ability of the different conditions. This study proposes a throughout evaluation of the biological activity (cell cytotoxicity, alkaline phosphatase activity, alizarin red mineralization test, and cellular adhesion). This broader approach was extended to different structures of the two morphologies (amorphous and crystalline, which were compared to as-received Ti samples) and an overall evaluation of their corrosion resistance behavior. Such a simultaneous study focusing on the different morphologies and structures is an effort to draw a new understanding of the best conditions for nanotubes to be used to design and implement high-performance, reliable medical implants. The two investigated morphologies have been chosen among several different attempts as they showed the highest potential during preliminary experiments. Thus, they were considered optimized layers in both electrochemical and *in vitro* biological responses, which we further evaluated in the present paper.

Materials and Methods
Sample Preparation
All specimens have been prepared from 2 mm thick, 14.3 mm diameter commercially pure Ti disks. Samples were ground with different grits of silicon carbide papers from P320 to 2400 before being polished with a 0.03 mm colloidal silica suspension. After polishing, the samples were cleaned in an ultrasonic bath for 10 min with deionized water, ethanol, and acetone. Lastly, they were rinsed again with deionized water and acetone and dried using compressed air.

The anodization was performed using a TCR-Electronic Measurements Inc. power supply that applied and controlled the desired potential between a large surface platinum gauze counter electrode and polished Ti disks as working electrodes, WE, with an exposed surface of 0.785 cm^2. For the sake of reproducibility, four samples were anodized simultaneously. They were assembled in

sample holders placed at the 3, 6, 9, and 12 o'clock positions regarding the circular cross-section of a cylindrical double-wall temperature-controlled cell. Only one side of each of the four WE were exposed to the anodizing solution. Sealing between solution and electrical connection is performed by a PTFE gasket. The counter-electrode was placed at the center of the cell in a position equidistant from the four WE to ensure a uniform and symmetrical current-lines distribution relative to each anodizing surface. As mentioned in the previous section, two optimized TiO_2 nanotubes morphologies were held according to their dimensions [13]: a small-diameter, ϕ short-length, l, layer (target values $\phi \approx$ 90nm, $l \approx$ 700nm), and a large-diameter, long-length one (target values $\phi \approx$ 130nm, $l \approx$ 5000nm). They are hereafter referred to as SS and LL, respectively, and were obtained from two distinct anodization protocols:

- SS: A constant voltage of 20 V for 1 h in glycerol, with 25 vol% of water and 0.25 M NH_4F electrolyte at 25º C.
- LL: A constant voltage of 60 V for 45 min in ethylene glycol, 7.5 vol% of water, and 0.25 M NH_4F electrolyte at 25º C.

The as-anodized samples presented an amorphous nanotube structure. Some samples were then submitted to two-hour annealing in air at 550 ºC to induce the TiO_2 crystallization into a mix of anatase and rutile that has been shown to be promising for biomedical applications [13].

Different samples were thus investigated throughout the present study. They are identified as SS_x and LL_x regarding their smaller or larger dimensions, with the subscript x standing for the structural identifier, amorphous (am), or crystalline (cr). For the sake of baseline comparison, the anodized samples' behaviors have been compared to polished, non-anodized, referred to as N-A, Ti disks.

Morphological, Structural, and Wettability Analyses of TiO_2 Nanotubes
The nanotubes morphology was characterized by scanning electron microscopy (SEM) using a Field Emission Gun Scanning Electron Microscope (FEG-SEM, ZEISS ULTRA 55), with an in-column secondary electron detector. An applied voltage of 3 kV was used to get higher spatial resolution.

The nanotubes structure was analyzed by X-Ray Diffraction (XRD) using the PANalytical X'PERT PRO MPD diffractometer, where a CuKa radiation (l = 1.5418 Å) was used. XRD scans were performed in the incident angle range 10º < 2Θ < 80º, with a step of 0.067º for amorphous samples and 0.033° for crystallized ones.

The wettability of the different layers was analyzed using a goniometer (Krüss, Model DSA 100). A 2μL deionized water drop was placed upon the samples' surface—fixed on a PTFE base—and the contact angle, Θ, measured after 5 seconds using a dynamic mode. Three samples were used for each morphology-structure type. The results were expressed as $\bar{\Theta} \pm \sigma_\Theta$, i.e., the average contact angles modulated by their respective standard deviations. GraphPad Prism program (version 5.01) (San Diego, CA, USA) was used to analyze the statistical differences with $p < 0.05$ being considered statistically significant.

Corrosion and Electrochemical Behavior in SBF

In order to have a more reliable evaluation of the different morphologies' suitability to be used as biomaterials, their electrochemical characterization was performed through polarization curves and electrochemical impedance spectroscopy, EIS, in Simulated Body Fluid (SBF),[30] pH 7.4, at 36.5 °C in the dark. A Gamry Reference 600 potentiostat was used to control a conventional three-electrode cell with the different Ti surfaces (exposed area 0.5 cm^2) as the working electrodes, a platinum grid as the counter electrode, and a Saturated Calomel Electrode (SCE) as the reference one. The different samples' overall corrosion behavior was evaluated through anodic potentiodynamic polarization curves measured at a scan rate of 0.5 mV s-1 from −0.03 to 1.5 V versus the open-circuit potential OCP. Steady conditions were ensured by a rest period of the samples immersed in the SBF electrolyte for one hour before the polarization curves were launched. The frequency-dependent electrochemical behavior was evaluated through potentiostatic EIS with a sinusoidal perturbation amplitude of 10 mV$_{rms}$ from 20 kHz to 20 mHz.

Cell Culture and Incubation During the Biological Analyses

The cell line was purchased commercially. For the *in vitro* tests, MG63 osteoblast-like cell lines (Rio de Janeiro Cell Bank, APABCAM, Rio de Janeiro, RJ, Brazil) were cultured in a-Modified Eagle's Medium (DMEM; Gibco-Life Technologies, NY, USA) supplemented with 10% fetal bovine serum (Gibco-Life Technologies, NY, USA), 100 U/mL penicillin (Gibco-Life Technologies, NY, USA) and 100 μg/mL streptomycin (Gibco-Life Technologies, NY, USA) in 75 cm^2 flasks (TPP, Biosystems, Curitiba, Brasil) and maintained in a humidified atmosphere with 5% CO$_2$ and 95% air at 37°C. The medium was changed every two days. Cultures were monitored daily using an inverted optical microscope (Carl Zeiss Microlimaging GmbH – Axiovert 40C, Germany). When confluent, cells were enzymatically removed and plated on the sterile samples in 24-well polystyrene plates (TTP, Biosystems, Curitiba, Brasil), at a density of 2×10^4 cells/well for a period of up to 14 days. Previously, the samples were sterilized in absolute ethanol and under an ultraviolet lamp for 3 hours. All tests were developed following the ISO-10,993-5 standard, as described in.[31] For all *in vitro* experiments, three independent experiments were realized (n=5).

Cell Cytotoxicity (MTT)

The cell cytotoxicity was evaluated following Mossmann,[32] using a colorimetric tetrazolium salt solution (MTT) assay (3-[4-dimethylthiazol-2-yl]-2, 5-diphenylte-trazolium bromide; thiazolyl blue) (Sigma Aldrich, St Louis, USA). Cells were cultured on the different titanium specimens for 1, 3, and 7 days and were distributed in 96-well microplates for viability experiments. After each time, the MTT solutions were added into each well (concentration of 0.5 mg/mL) at 37°C and kept for 4 hours to form purple formazan crystals. Next, the supernatant was removed, followed by the addition of 1 mL dimethyl sulfoxide (DMSO –1 Sigma Aldrich, St Louis, USA) to each well. The plates were then stirred on a plate shaker for 20 min to dissolve the formazan crystals. 200 μL of this solution was transferred to a well plate for colorimetric analysis.

The resulting optical density (OD) reading was measured in a spectrophotometer (Biotek-EL808IU, BioTek Instruments, Winooski, VT, USA) at 570 nm, and the data normalized by the control group (N-A samples). This assay is versatile and quantitative, being a powerful technique for cytotoxicity assays. The amount of formazan produced in the MTT reaction is vital in evaluating metabolically active cell group proliferation and survival. Activated cells produce more formazan, which allows measurement of activation even in the absence of

proliferation. These properties are related to active mitochondria.

Alkaline Phosphatase Activity (ALP)

Functional mineralization of alkaline phosphatase was evaluated after cell incubation for five days on the different samples. This activity was assessed using the hydrolysis of thymolphthalein monophosphate substrate following the manufacturer's recommendations (Alkaline phosphatase activity 40, Labtest Diagnóstica, Belo Horizonte, BR). The absorbance was measured by spectrophotometer (Shimadzu Europa GmbH UV 1203) with substrate added to each well, and the standards were prepared to be read on a microplate reader at 590 nm. The ALP activity was standardized using total protein level, and the data were presented as μmol of activity per well according to the values obtained from a standard curve. Values were presented in μmol of thymolphthalein/h/mg of protein.

Alizarin Red Staining (ARS)

For the alizarin red mineralization test quantitative analysis of mineralized matrix nodules, the cells were cultured for 14 days on samples, washed with Hank's solution (Sigma Aldrich, St Louis, USA) at 37 °C, and fixed with 70% ethanol for 1 h at 4 °C. Following fixation, the cells were stained with 2% Alizarin red S (Sigma Aldrich, St Louis MO, USA) for 15 min at 37 °C. The dye was then extracted according to the colorimetric method previously described in,[31] and the absorbance was measured by spectrophotometer (EL808IU Biotek Instruments, Winooski, USA) a wavelength of 405 nm. The values were expressed as OD.

Data were submitted to one-way analysis of variance (ANOVA) followed by a Tukey's test, which was used for multiple comparisons. GraphPad Prism program (version 5.01) (San Diego, CA, USA) was used, and a value of p<0.05 was considered statistically significant.

Cellular Adhesion

MG63 cells lines (Rio de Janeiro Cell Bank, APABCAM, Rio de Janeiro, RJ, Brazil) were seeded on the scaffolds at a density of 5000 cells/cm^2 and cultivated for one and three days. After each time, the samples were washed in PBS (three times) to remove non-adherent cells. Then, samples were chemically fixed in paraformaldehyde (4%) at room temperature (20 min). Afterward, an ascending series of ethanol

was used to dehydrate the samples (10, 30, 50, 70, 90, and 100%). Before characterization, a thin gold layer was sputtered onto the scaffolds. Then, cells were stained using trypan blue (Sigma-Aldric) and counted using a Cell Counter (Countess®, Invitrogen). All results were expressed as mean using the total cells for each group. Cellular adhesion and proliferation were further evaluated by FE-SEM (Zeiss - EVO MA10).

Results

Structural Analysis of TiO$_2$ Nanotubes

Figure 1 presents XRD patterns of morphologies SS and LL in both conditions, as-anodized and after heat treatment in air at 550 ° C for 2 h. The XRD pattern of the non-anodized Ti substrate (N-A) is also depicted for comparison and indicates a pure hexagonal α-Ti structure (Figure 1A). The XRD spectra of the nanotubes of both morphologies before heat-treatment, SS$_{am,}$ and LL$_{am}$ in Figure 1A, present only diffraction peaks associated with the α-Ti substrate confirming that both as-anodized oxide layers are amorphous.

As expected, the heat treatment induced the crystallization of the amorphous layers into a mix of anatase and rutile as indicated by the presence of their respective peaks, Figure 1B. The higher intensity of the peaks reflected from sample LL$_{cr}$ is related to the larger volume and mass of crystalline phases in the longer and larger nanotubes morphology.

Results in Figure 1 are consistent with the well-known route for TiO$_2$ crystallization proposed in the literature. At annealing temperatures around 280°C–300°C, crystallization towards the anatase structure[12,33] is initiated at the nanotubes' base, via interfacial nucleation, due to the available larger space for crystal growth than in the tubes' walls.[12] The nanotubes are then crystallized into anatase. Above 430°C–550°C, the anodized layer adopts a hybrid structure where the nanotubes retain the anatase structure while the barrier layer at the metal|NTs interface is transformed into rutile.[25,34] Such an observation was confirmed by electron energy loss spectroscopy (EELS) in.[25] The rutile phase's appearance is mainly due to the thermal oxidation of the Ti substrate, which leads, within this temperature range, to the formation of TiO$_2$ in rutile form.[13] As the annealing temperature increases, the rutile barrier layer thickens, fed by the nanotubes' bottom.[35]
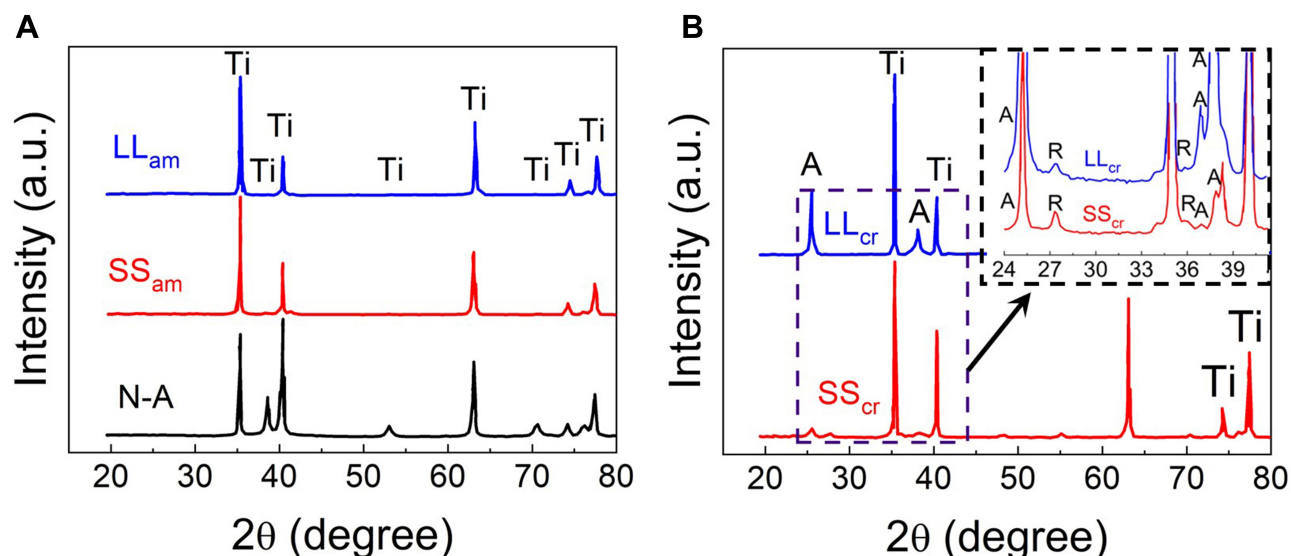
Figure 1 XRD patterns of different samples: (**A**) not-anodized, N-A, and as-anodized SS$_{am}$ and LL$_{am}$ and (**B**) annealed in air at 550 ° C for 2 h (SS$_{cr}$ and LL$_{cr}$). In the inset: zoom at 24° < 2Θ < 42° indicating the crystallization of both morphologies into a mix of anatase (A) and rutile (R).

Morphological Characterization of TiO$_2$ Nanotubes

Figure 2 gives an overall view of the different nanotubes' morphologies. Regarding the as-anodized samples, SS$_{am}$ layers (Figure 2A and B) were composed of short ripple-walled (usually referred to as bamboo-like) slightly interspaced nanotubes. On the other hand, LL$_{am}$ (Figure 2D and E) grew in a close-packed frame of long flat-walled tubes. The heat-treated samples SS$_{cr}$ (Figure 2C) and LL$_{cr}$ (Figure 2F) did not show any significant morphological changes. This is in line with some previous findings in the literature,[36] which reported that,
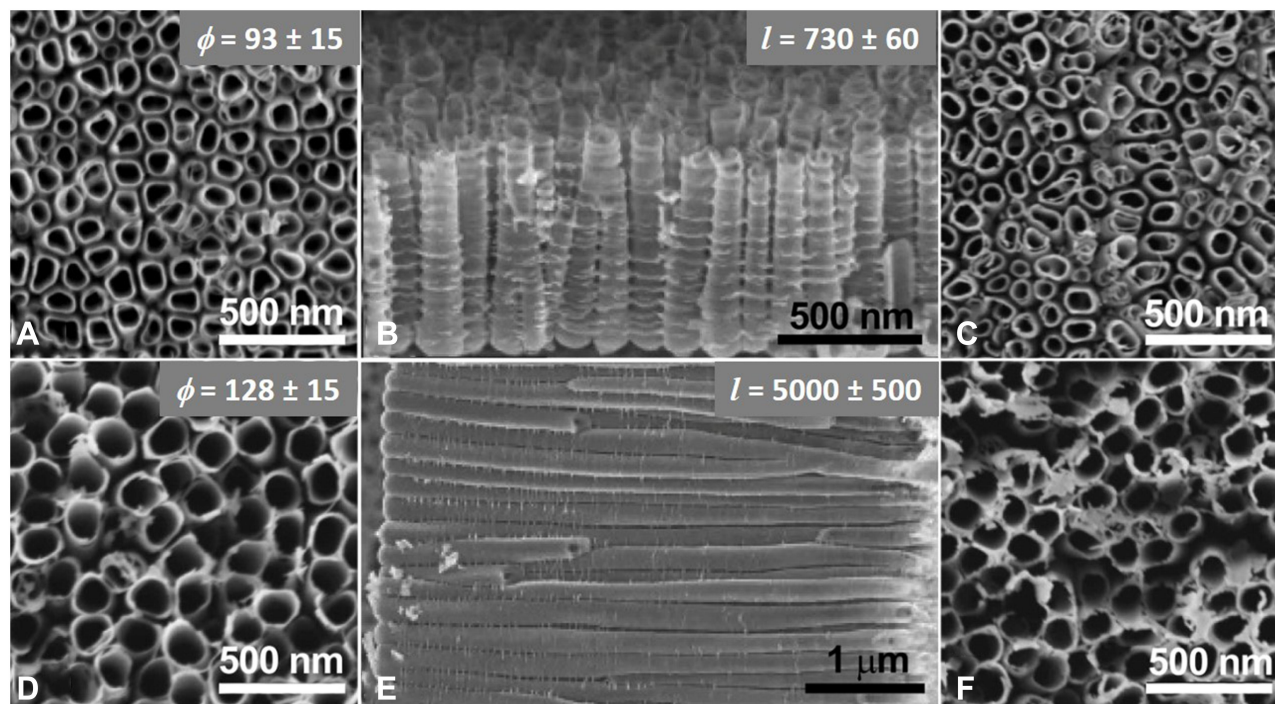

Figure 2 SEM images of the different TiO$_2$ nanotubes morphologies according to anodizing protocols SS (**A–C**) and LL (**D–F**). As-anodized samples: SS$_{am}$ top (**A**) and cross-section (**B**) views and LL$_{am}$ top (**D**) and cross-section (**E**) views. Annealed in the air at 550 °C for 2 h: SS$_{cr}$ (**C**); LL$_{cr}$ (**F**). Dimensions in nm expressed as $\bar{x} \pm \sigma_x$.

672

International Journal of Nanomedicine 2021:16

when annealed in air, nanotubes morphologies are stable up to 580 °C.

From the perspective of the wide use of this kind of surface modification in biomedical materials, an important remark concerns the high reproducibility of the anodizing protocols SS and LL described in Sample Preparation. Indeed, as indicated in Figure 2, the dimensions of both morphologies perfectly matched the target values associated with the anodizing protocols.

In which concerns the heat treatment-induced crystallization of the anodized layers, the literature[25,37,38] showed that the nanotubes tend to preponderantly crystallize into anatase phase, while the dense barrier layer at the nanotubes/substrate interface crystallizes into rutile. This crystallization profile seems to be confirmed by the XRD pattern in Figure 1, as the relative intensities of the large surface anatase-nanotube peaks are much more pronounced than those of the underneath thinner dense rutile layer for both SS and LL morphologies.

It is also worth noticing that the heat treatment can modify the interface between the substrate and the nanotubes. Figure 3 depicts the cross-section of different nanotubes layers before and after annealing. They clearly show a dense oxide layer of about 100 nm developed during the annealing at the nanotubes layer's bottom. Indeed, under the effect of temperature, the thin dense barrier layer

formed during the anodization (Figure 3A) tends to grow thicker (Figure 3B and C). This tendency increases with temperature, leading to an overgrowth of the dense layer and eventually impairing the nanotube layer structure, potentially impacting its bioactivity. However, as shown in Figure 3, the heat treatment conditions applied in the present study did not promote the growth of the interfacial oxide into too thick barrier layers. Indeed, although thicker than the amorphous layer before annealing (ca 10 nm, Figure 3A), the annealed dense layers remained considerably thin (90–110 nm thick, Figure 3B and C) compared to nanotubes' length in both SS_{cr} and LL_{cr} samples. These results indicate that the morphological integrity of the nanotubes was preserved after heat treatment since it did not entail any significant change of the nanotubes dimensions (diameter, length, wall thickness, …), nor any defects in the layer structure as fractures, delamination, or voids at the metal-nanotube layer interface. This is an important point as degradation and morphology changes have been reported for higher temperature annealing (> 600 °C).[39]

Corrosion and Electrochemical Behavior

Figure 4 presents the typical potentiodynamic polarization behavior in SBF for all the different morphologies, thus allowing the straightforward comparison between non-
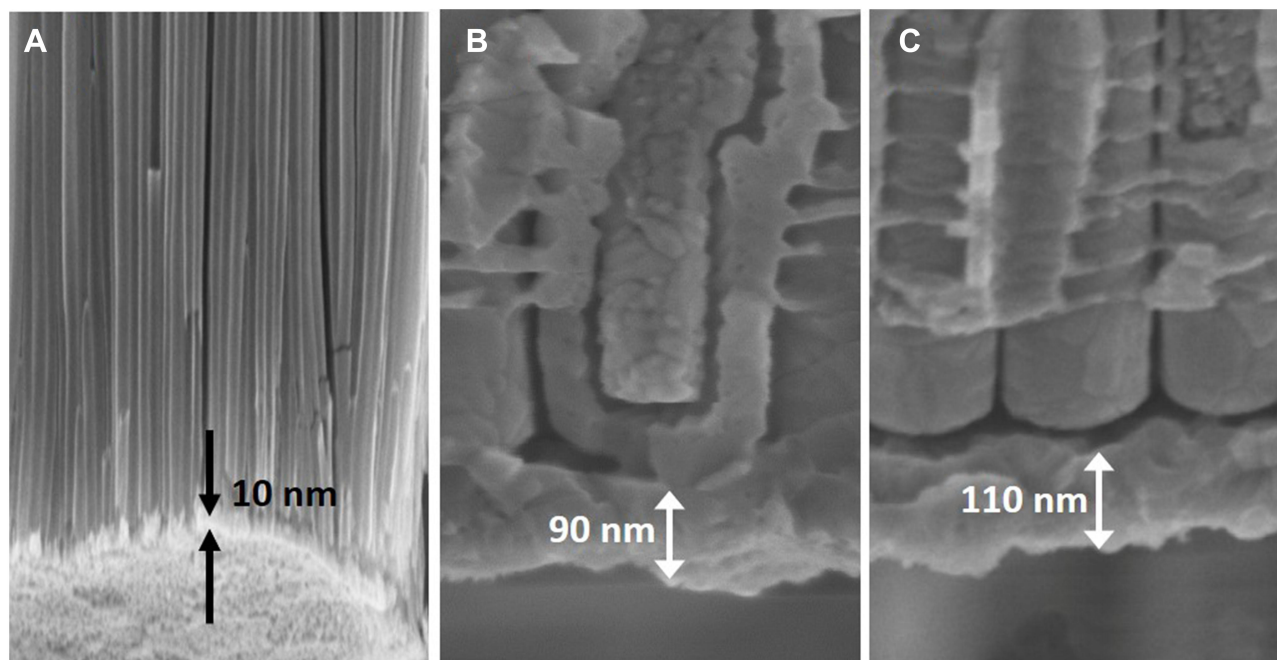
Figure 3 SEM images of the dense interfacial layer (**A**) before annealing, a thin dense layer formed during anodization beneath the nanotubes, SS_{am} layer; and in samples annealed in air at 550 °C for 2 hours: (**B**) SS_{cr}; (**C**) LL_{cr}. In the inset: Black and white arrows showing the thickness.
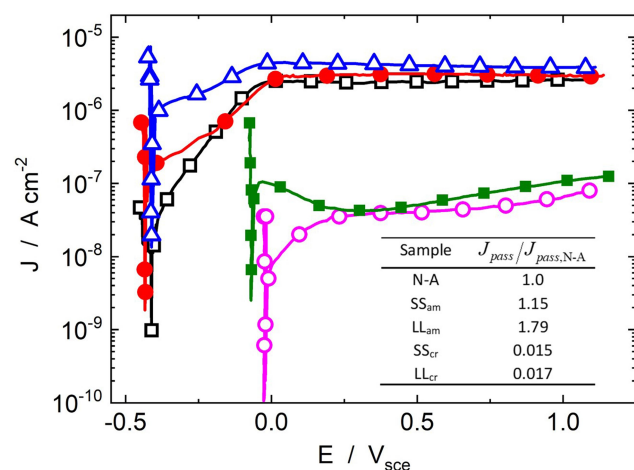
Figure 4 Potentiodynamic polarization curves in SBF electrolyte at 36.5 °C at a scan rate of 0.5 mV s^{-1}. Cell kept in the dark: (□) N-A; (●) SS$_{am}$; (▲) LL$_{am}$; (○) SS$_{cr}$; (■) LL$_{cr}$, In the inset: Passivation current densities, J_{pass}, normalized against the non-anodized sample, $J_{pass,N-A}$.

anodized, SS, and LL samples in both as-anodized and heat-treated conditions.

Although not conveying intrinsic kinetic information as does the corrosion current density, the corrosion potential, E_{corr}, allows a first meaningful screening of the different behaviors. Indeed, E_{corr} gives a good indication of the various systems' nobility and stability in the investigated medium. In this sense, it is worth noticing that the anodization process itself had almost no effect on the metal | electrolyte redox behavior since the E_{corr} of all the amorphous samples, as-anodized, SS$_{am}$, and LL$_{am}$, were nearly the same as the one of the non-anodized sample, N-A. In a preliminary approach, these invariable values might be related to the fact that these different interfaces' chemical nature did not change with anodization. Indeed, the non-anodized sample is already recovered by a thin amorphous layer of TiO$_2$. Even though the anodized samples have highly developed surfaces, they are formed by roughly the same chemical—and still amorphous as shown by the XRD in Figure 1—compound. This chemical uniformity is likely to pin the respective E_{corr} values, even more since the electrochemical potential is an intensive quantity not straightforwardly dependent on the developed surface.

However, unlike the anodization, the heat treatment and the consequent nanotube layers crystallization entailed a significant modification of the surface, which reflected in a remarkable increase of E_{corr} (> 0.4V). Once again, however, no significant difference was observed between the SS and LL morphologies, which reinforces the idea that much more than the developed surface, the layer's nature/

structure controls the metal | electrolyte interface. Therefore, as far as E_{corr} can indicate, the crystallized structures constitute nobler and more stable interfaces when immerged in the SBF electrolyte. The main physical reason behind this steep increase in E_{corr} is likely related to the heat treatment-induced thickening of the dense layer underneath the nanotubes (cf Figure 3).

Regarding the evolution of the corrosion current density, J_{corr}, which is straightforwardly related to the corrosion rate, it must be stressed that the unambiguous and precise determination of J_{corr} values is a difficult task very often overlooked. Indeed, from a strict point of view, the Tafel extrapolation—one of the most widely used technique to estimate J_{corr}—is only pertinent if the kinetic behavior described by the current evolution around E_{corr} is linear through at least one decade in the logarithm space. In many—if not most—experimental corrosion studies, however, the linear evolution of the current is limited to a narrow segment, thus precluding the precise estimation of J_{corr}. This truncated linear behavior was also the case for almost all the curves in Figure 4. Therefore, for the sake of rigor, the corrosion current density is analyzed in a semi-quantitative approach only, which largely suffices in the framework of the present study. Indeed, all the curves show low or very low current values that did not indicate any significant dissolution in any morphologies or experimental conditions. At the same time, the curves are different enough for a neat hierarchy to be established between the different samples in terms of their electrochemical stability in the SBF electrolyte.

The overall analysis of the polarization curves in Figure 4 reveals that, as observed before,[40,41] the samples' behavior is characteristic of a passive state in SBF. In fact, for all samples, a current plateau is established over a wide range of potentials, corresponding to a current limitation due to mass and charge transport through the dense barrier oxide layer.[42] This scenario is consistent with the only moderately aggressive electrolyte. Thus, whether or not covered by nanotubes, the specimens are already passive yet at the corrosion potential, allowing Jcorr to be assimilated to the current density of the passivation plateau, Jpass in.[42,43] To better illustrate the impact of both the anodization process and the heat treatment-induced crystallization of the nanotubes layers on the different specimens' kinetic behavior, the passivation current densities are given in the inset of Figure 4, normalized against the non-anodized behavior. The values clearly indicate that, while the anodization alone did not entail a significant

change in samples' behavior than the non-anodized condition, the heat treatment, and the induced crystallization did have a highly positive effect on the electrochemical behavior of both SS_{cr} and LL_{cr} morphologies. Besides a much higher E_{corr} as discussed before, Figure 4 also shows that, regardless of the overpotential, the current densities measured with the heat-treated samples were almost one hundred times lower than those measured with non-annealed samples. This remarkable effect of the heat treatment on the electrochemical response of SS_{cr} and LL_{cr} samples is likely to be due to the thickening of the dense rutile layer, as seen in Figure 3. Located at the substrate/nanotubes interface, this dense layer modulates the interactions between the metallic substrate and the electrolyte at the nanotubes' bottom. For amorphous nanotubes, as seen in Figure 3A and also reported in the literature,[25,44] this interfacial layer is relatively thin and can even detach from the bottom of the nanotubes.[44] In this situation, the nanotubes could even facilitate the electrolyte's access to the metal/oxide interface, allowing localized corrosion to take place, as pitting. Conversely, the heat treatment favors the thickening and the intimate merger of the barrier layer with the bottom of the nanotubes to form a compact and thick layer, Figure 3B and C, thus further protecting the metal from corrosion.

This layered-complex structure was also evaluated through EIS, and the results are present in Figure 5. The typical Nyquist plots after anodization and annealing depict a truncated high-frequency capacitive behavior that evolves to a straight line at middle-low-frequencies. This behavior is the overall outcome of a highly distributed frequency response which cannot be modeled by a conventional R-L-C electrical equivalent circuit, EEC, and which was associated to the different contributions from the overall interface structure: 1) external nanotube layer; 2) the bottom of the nanotubes combined with the dense layer; 3) the modified electrolyte inside the pores; and 4) the interface itself, where the charge transfer reactions take place. This complex structure has been successfully modeled with a modified transmission line model with anomalous (for frequency-dependent) transport behavior represented by the EEC, also displayed in Figure 5. The first advantage of this model is that it makes explicit the role of the dense layer at the bottom of the structure, with a constant-phase element (a non-ideal capacitance), Q_b, from which the thickness of the dense layers was estimated and shown to be in good agreement with the
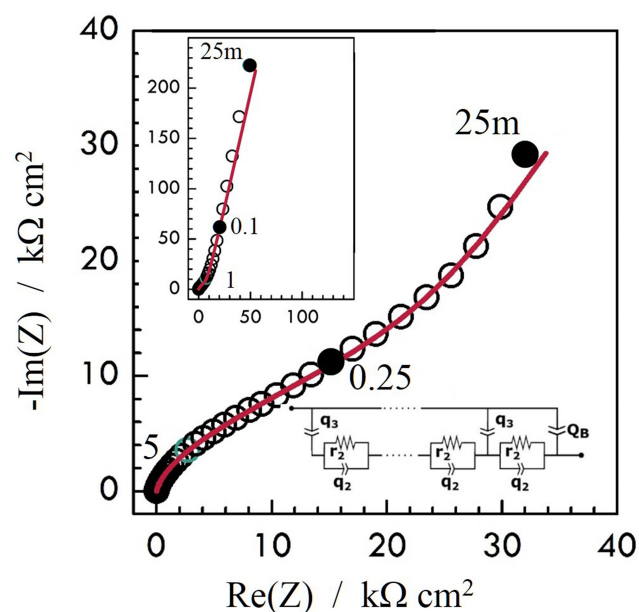

Figure 5 Nyquist plot of experimental (symbols) and fitted (solid lines) impedance spectroscopy of annealed layers LL_{cr} (main plot) and SS_{cr} (upper inset) measured in SBF electrolyte at open circuit conditions, 36.5 °C, in the dark. Frequencies in Hz. Bottom inset: Electrical equivalent circuit based used for fitting the experimental diagrams. q_2 and r_2 represent the nanotube solid channel's internal distributed resistance and non-ideal capacitance, q_3 the nanotube's wall interfacial capacitance, and Q_b the non-ideal dense layer capacitance.

measurements obtained from microscopy imaging as in Figure 3.

Another interesting point raised by the EIS modeling is that the distributed internal resistances inside the nanotube channel, r_2, are different depending on the size of the nanotubes, indicating that the longer LL_{cr} layer is more defective than the smaller SS_{cr} one, which can eventually impact the nanotube layer wettability as discussed in the next section. The full EIS investigation of the different nanotubes layers, as well as the development of the modified transmission-line model, can be found in Ref.[21]

Wettability Analyzes

Surface wettability is a crucial parameter to improve biological responses such as protein adsorption and blood coagulation, as well as osteogenic properties (bone remodeling). Some authors also related surface hydrophilicity to the rate of cell spreading, osteoblast differentiation, and improvement of metabolic activity.[45–47] Figure 6 summarizes the wettability properties of each condition compared to the non-anodized one. All samples presented contact angles far below 90° (20° $<\Theta<$ 65°), thus indicating a hydrophilic behavior[48] regardless of the morphology and treatment applied. The nanotubes morphology (SS or
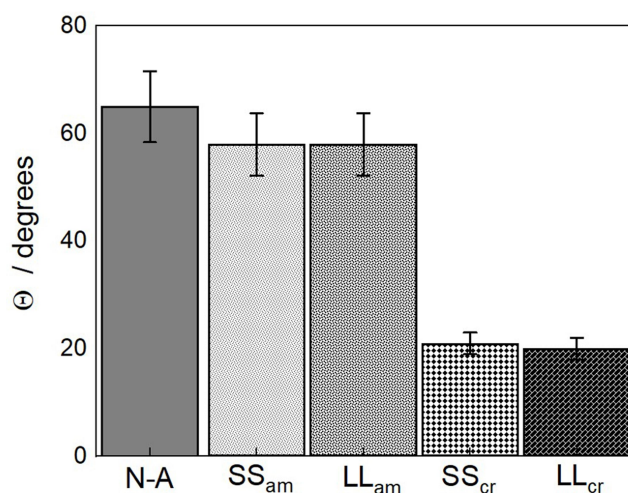
Figure 6 Wettability analysis of the different samples using contact angle analysis. Results were expressed as $\Theta \pm \sigma_\Theta$. Statistical differences were analyzed using GraphPad Prism with p<0.05 considered statistically significant.

LL) had no impact on the wettability since, for the same crystallographic structure, amorphous or crystalline, the angle values were identical or very similar with no significant scattering. As it was already the case for the electrochemical responses, the main change in the wettability was again related to the heat treatment that induced a substantial decrease in the contact angle of the crystallized structures (ca 20º) compared to both N-A (ca 65º) and amorphous samples (ca 58º). This decrease in the contact angle can be ascribed to a higher content of the anatase phase in the nanotube layer after heat treatment (see Morphological Characterization of TiO2 Nanotubes), as reported in the literature.[45,49,50] Other possible explanations are related to the annealing inducing a higher defective structure as raised by the EIS measurements, mainly the presence of oxygen vacancies that can trap water molecules creating a high surface density of hydroxyl groups[51] and also to the removal of organic contaminants induced by the annealing.[52]

Biological Assays

Hydrophilic materials with high corrosion resistance are expected to be fit for bone tissue engineering applications. As seen in the previous section (cf. Figures 4–6), the different surfaces seemed to satisfy these criteria. Particularly, the heat treatment-induced crystallization allowed the formation of nanotube layers with very low corrosion current densities as well as low contact angles in the wettability test. A major question remained, however, related to their ability to favor protein adsorption

promoting viable nucleation of osteoblasts. Therefore, one of the present study's main objectives was to verify whether the development of those nanotubes-layered surfaces of different topographies and crystalline structures would also be compatible with osteoblast's viability, growth, and proliferation.

In this sense, the comparative evaluation of the cell viability on non-anodized and anodized samples was carried out through a MTT colorimetric assay according to OD values at 570 nm.[53] The MTT can assess the cell metabolic activity of the NAD(P)H dependent cellular oxidoreductase enzymes related to active mitochondria so that the reaction reflects the number of viable cells present on the surface.

The MTT cell viability test results with tetrazolium salts performed from cell incubation and after 1, 3, and 7 days of cell culture are shown in Figure 7. A first remark is that the amount of formazan produced in the MTT reaction is essential in evaluating metabolically active cell group proliferation and survival. The cytotoxicity test result indicates that all groups, including the non-anodized samples N-A, showed increased cell viability with time. Nevertheless, no matter how long the cell culture was, the number of viable cells was more extensive in nanotube layers than N-A surfaces. In which concerns cell proliferation, in all evaluated periods, samples SS and LL, regardless of their structure, amorphous or crystalline, showed statistically significant (p <0.0001) increased cell viability, and a proliferation increase rate between 1 and 7 days
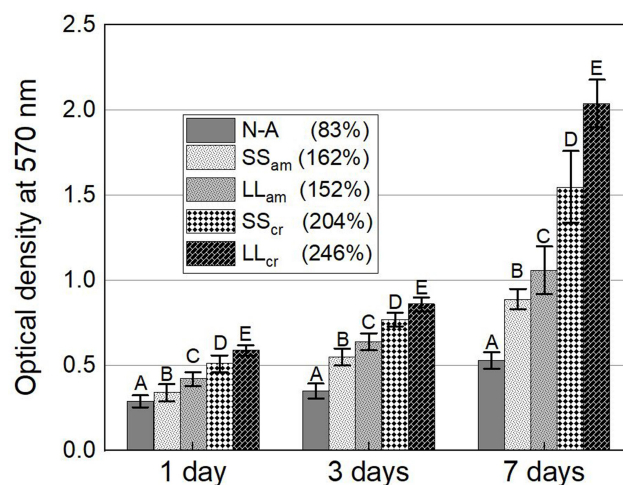

Figure 7 Cell cytotoxicity (MTT assay) at 1, 3, and 7 days of cellular culture. Values reported as $\overline{OD} \pm \sigma_{OD}$ (n=5). Letters indicate significant differences for p<0.05. Values (%) in the legend correspond to the cell proliferation increase rate between 1 and 7 days for the different samples.

much higher—between ca 150% and 250% as depicted in Figure 7—than the one for N-A substrates (83%).

The comparison between the nanotubes-layered groups brings the same qualitative trend already identified in the electrochemical responses and wettability tests, i.e., better performance of the heat-treated crystallized groups. The anatase-rutile crystalline structure seems to improve cell viability, illustrated by the higher OD values for samples SS_{cr} (201.33% of counts increase in seven days) and LL_{cr} (251.98%) than for SS_{am} (158.33%) and LL_{am} (148.67%).

Finally, a clear differentiation between the two crystallized conditions SS_{cr} (201.33%) and LL_{cr} (251.98%) appear at the last stages of the test, by one week of cell culture. This significant difference in the final OD values points to a synergistic effect between the mixed anatase-rutile structure and the high specific surface allowed by the larger nanotubes morphology that, combined, seems to have allowed an enhanced cell activity. These results show the possibility of tuning the properties of TiO_2 nanotubes layers, thus further generating materials with enhanced anodized morphology.

The ALP activity of MG63 osteoblast-like cell lines on the different samples was measured based on their total protein content (Figure 8). ALP activity increased gradually with the incubation time, thus indicating the maturation of MG63 cells through this period.[31] As clearly seen in the figure, after five days of cell culture, all nanotubes-layered surfaces showed an increase in ALP activity compared to the non-anodized ones. Once again, the results indicate a positive effect of the heat-treatment as the
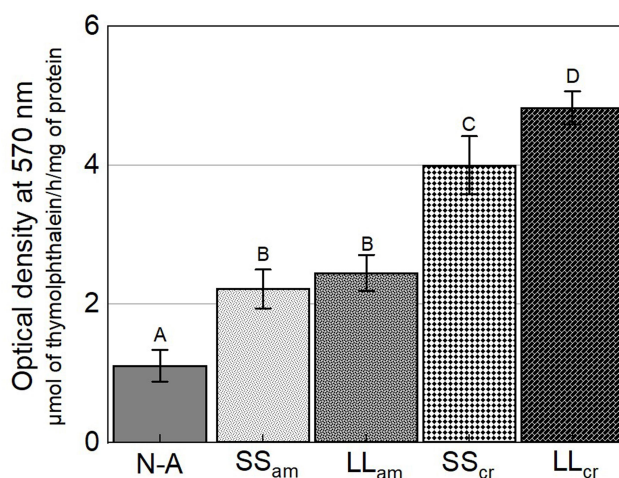
MG63 cells presented a statistically significant increase ($p < 0.0001$) of their alkaline phosphatase activity when cultivated on SS_{cr} and LL_{cr} samples compared to both non-anodized and non-heat-treated groups. This better performance of the heat-treated samples is likely related to the preferential presence of anatase in nanotubes' structure, as discussed before. Concerning the nanotubes dimensions, the larger layers, LL_{cr}, seemed to favor higher cellular viability that can facilitate the osteogenic process.

Functional mineralization was observed as a marker of osteogenic differentiation from the production of osteoblasts in contact with the different samples, as illustrated in Figure 9. After the ARS extraction, however, the anodized samples presented much higher concentrations—OD, 0.69, and 0.78, for SS_{cr} and LL_{cr}, respectively, as seen in Figure 10 than the N-A group OD 0.28. Even though there was no statistically significant difference ($p > 0.05$) between the heat-treated SS_{cr} and LL_{cr} themselves, they presented significantly higher values of ARS ($p < 0.0001$) than SS_{am} and LL_{am}, exhibiting higher mineralized matrix formation.

MG63 cells adhesion on the different surfaces was also evaluated after 1 and 3 days (Figure 11). Only healthy cellular behaviors were observed without characteristic footprints of cytotoxic cellular changes, such as pyknotic nuclei, fragmented cytoplasm, or with granulation. Well, adhered and dispersed MG63 cells were observed after one day for all groups. After three days, however, samples SS_{cr} and LL_{cr} presented a higher density of cells that freely spread, developing extensive filopodia and lamellipodia. This faster growth profile is consistent with the higher proliferation rate observed in the different assays for cells cultivated on annealed structures, as seen in Figures 7–10. These results are likely to be related to the enhanced hydrophilic behavior of crystalline layers, as indicated by the lower wettability angles depicted in Figure 6, which, in turn, may have improved the cell adhesion properties.

Discussion

In which concerns the biological assays, the first critical comment is that none of the tested samples induced cytotoxic effects in MG63 cells during the incubation period. Conversely, the experimental results showed that optimized nanotubes with appropriate morphology and structure could be considered a highly suitable surface modification treatment to be used in biomaterials.

Starting with the MTT test, considered as an indicator of the cell growth on biomaterials,[32] results showed that
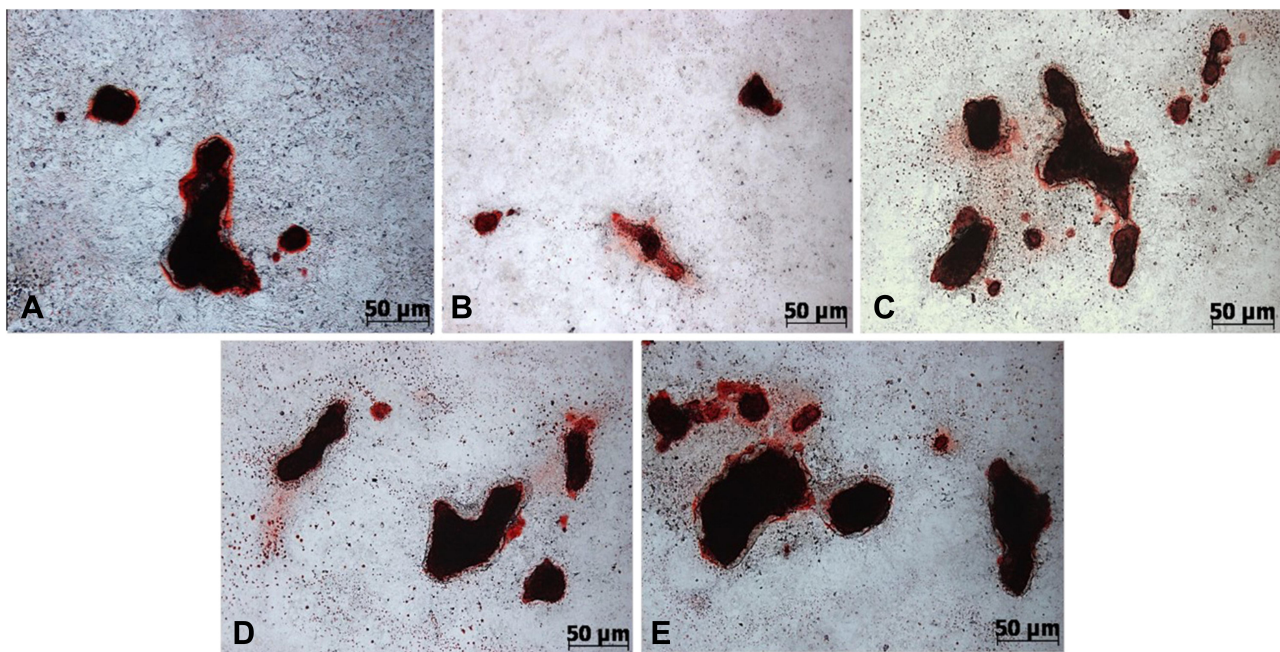

Figure 8 Alkaline phosphatase activity after five days of MG63 cellular culture. Values were reported as $\overline{OD} \pm \sigma_{OD}$ (n=5). Letters indicate significant differences for $p < 0.05$.

Figure 9 Alizarin red staining of mineralized nodule formation *in vitro* after 14 days. (**A**) N-A; (**B**) SS$_{am}$; (**C**) SS$_{am}$; (**D**) SS$_{cr}$; (**E**) LL$_{cr.}$
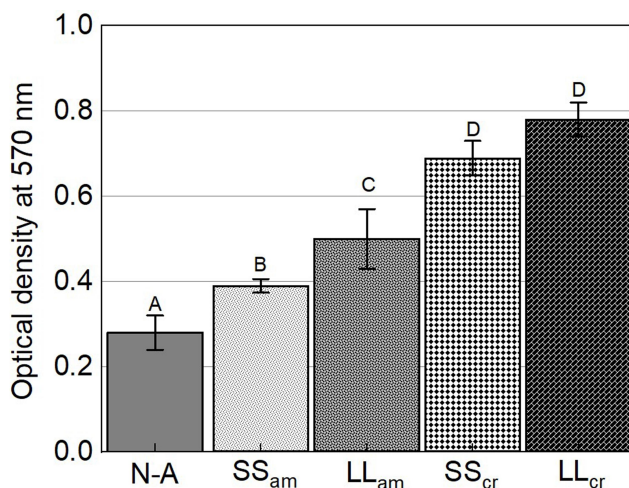

Figure 10 Alizarin red staining after 14 days of cellular culture. Values reported as $\overline{OD} \pm \sigma_{OD}$ (n=5). Letters indicate significant differences for p<0.05.

the increase in cell viability was proportional to the period of culture and that the groups with nanotubular TiO$_2$ layer yielded better results than the non-anodized one (Figure 7). The biological response was thus dependent on the biomaterial's surface characteristics, as reported by Kim et al,[54] who observed a proportional relationship between surface roughness and cell viability.

The ALP test is an indicator of osteoblast differentiation and maturation.[31,55] The nanoscale surface topography positively influenced the osteoblastic maturation since

the nanotubes-layered groups showed ALP values at least twice the one from the non-anodized surfaces. Indeed, it appeared that the only presence of the nano-structures, regardless of their microstructure, resulted in higher cellular bioactivity.[56] Nevertheless, as seen in Figure 8, the crystallization induced by the heat treatment with the consequent increase of anatase proportion in the nanotube structure (cf Figure 1B) yielded a boosted cellular activity. These results are in line with previous results from Chen et al,[28] indicating that the anatase phase of titanium with nanoscale topography yields the best biological effects for cell adhesion, spreading, proliferation, and differentiation. There are, therefore, strong therapeutic prospects for this biomaterial film for osteoblast proliferation, with possible applications for orthopedic and dental implants.

Alizarin red staining is an indicator of calcium production by mature osteoblastic cells with consequent mineralization of the extracellular matrix.[28] Higher calcium concentrations with the formation of mineralized nodules were found in the groups with a nanotubular surface in relation to the non-anodized group. In all the tests, it was possible to observe the positive influence of the samples' surface topography with nanostructured oxide layers and, as before, an enhanced response from crystalline layers (Figures 9 and 10).

The ensemble results presented here clearly indicate that the anodization protocol applied brought unequivocal
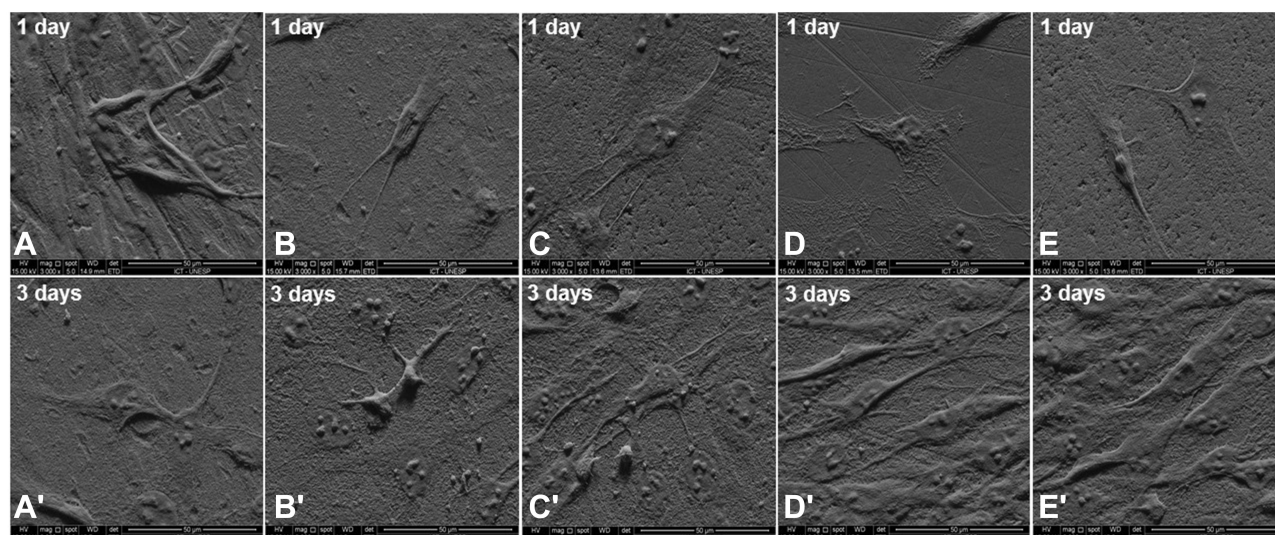
Figure 11 FE-SEM micrographs of MG63 cells cultivated on samples after 1 and 3 days of incubation. (**A, A′**) N-A; (**B, B′**) SS_{am}; (**C, C′**) LL_{am}; (**D, D′**) SS_{cr} and (**E, E′**) LL_{cr}.

benefits to the biomaterial | biological-media interface, be it from physicochemical or biological points of view. It is worth stressing that these positive effects are unambiguously built-up in two steps, or, in other words, two complementary levels. In the first, the nanotubes' growth induces the development of a huge specific surface area between the biomaterial and the cells. A geometrical model allowed the estimation of the nanotubes layers' developed surface area as 30 cm^2 and 140 cm^2 per projected square centimeter for samples SS and LL, respectively. Details on the estimation procedure can be found in Hilario et al[21] and references therein. This highly developed surface intrinsically stimulates interactions between the nanotubes surface and the culture media, thus favoring cell adhesion and proliferation.[57] Our results fully corroborate this trend in good agreement with previous studies where the authors reported more significant cell proliferation on micro and nanostructured surfaces than on smooth surfaces.[2,58,59]

Nevertheless, the benefits brought by the surface development alone had limited reach. Indeed, the second step in the build-up of an optimized nanostructured layer consisted of a heat treatment that, while keeping the nanolayer unmodified from a topographical point of view, clearly enhanced all the investigated properties. From the electrochemical responses (Figures 4 and 5), through the wettability behavior (Figure 6) till the different biological tests (Figures 7–11), the crystallization of the nanotube layer in a preponderant anatase phase structure triggered an overall improvement of the surface properties that ultimately reflected in their biological interactions. More specifically, the crystallized groups SS_{cr} and LL_{cr} have systematically shown better responses in cell viability and proliferation (Figure 7), differentiation (Figure 8), mineralization (Figures 9 and 10), and cellular adhesion (Figure 11).

Considering that the heat treatment did not impact the nanotubes' integrity either their morphology, this vast and significant improvement of the different surfaces' properties must be ascribed to the phase transformation from amorphous to anatase-based nanotubes. This conclusion is supported and confirms previous studies in the same line. Recently, Khrunyk et al showed that the crystalline TiO$_2$ nanotubes increased the adhesion, growth, and osteogenic differentiation of osteoblasts cells.[60] Chen et al[28] biologically evaluated the three phases of TiO$_2$ (rutile, anatase, and amorphous titania) and reported that the anatase phase showed better bioactivity in cell adhesion, proliferation, and differentiation. In a similar study, An et al[61] individually evaluated the rutile, anatase, and amorphous titania phases and a mix of the rutile and anatase phases. They found higher levels of cellular bioactivity in the anatase and rutile mix than in the individual phases.

The different experiments indicate that the heat-treated, larger dimensions nanotubes layer appear as a potential surface modification treatment for dental and orthopedic implants after being validated by *in vivo* tests. Indeed, the better results generally presented by LL_{cr} in comparison to SS_{cr}, are much certainly an effect of the synergistic interplay between the anatase-rich crystalline phase and the higher specific surface area developed by larger nanotubes.

In a more objective insight into this improved behavior, these results can be ascribed, from a qualitative point of view to a better wettability (cf Figure 6) induced by an anatase-rich crystalline structure of the layer supposed to be richer in defects as oxygen vacancies that can enhance the hydrophilic surface character, which is consistent with the results from the EIS modeling (cf Figure 5). This change in the interface's nature/structure may be quantitatively boosted thanks to increased interactions between cells and the developed surface (cf Figures 7, 8 and 10).

A final critical remark concerns the substantial enhancement of the corrosion resistance and the overall passivation behavior of the crystalline samples SS_{cr} and LL_{cr}, thanks to the heat treatment of the pre-anodized samples (Figure 4). This is another significant improvement since a highly reactive surface from an electrochemical point of view might induce continuous surface modification, layer delamination, and, worst, the potential release of toxic elements, thus seriously jeopardizing the benefits achieved from a biological point of view.

Conclusion

In this study, we analyzed the corrosion behavior and biological activity of two different anodized nanotubes' morphologies (Long and Larger [LL], Shorter and Smaller [SS] having two different structures (amorphous [am] and crystalline [cr]). Comparison of bioactivity was made regarding Ti substrates. After analyzing and discussing the results, the following conclusions can be drawn:

- The thickening of a dense rutile layer underneath nanotubes induced by crystallization heat-treatment substantially enhanced the corrosion resistance and the crystalline samples' overall passivation behavior.
- As observed in corrosion analysis, surface properties were improved by the crystalline state of anodized samples, thus also influencing biological activity. Such an influence was observed in the contact angle of wettability tests, which were remarkably lower in crystalline samples than in other conditions.
- Contact angles decreased in the sequence of Substrate, SS_{am}, LL_{am}, SS_{cr}, and LL_{cr}. The better wettability appeared to have a synergistic effect with the highly developed surface of the crystallized LL_{cr} samples that favored cell proliferation and adhesion. The annealing procedure is likely to have induced a more defective structure with a higher density of oxygen vacancies that would enhance the

LL_{cr} surface's wettability. Therefore, all biological responses were improved in the same sense, i.e., mineralization and induced cellular activity, MG63 cells alkaline phosphatase activity, and mineralized matrix formation enhanced from the Substrate, SS_{am}, LL_{am}, SS_{cr}, to LL_{cr}.

Data Sharing Statement

All raw data from characterization are available from the corresponding author upon request.

Author contributions

All authors made a significant contribution to the work reported, whether that is in the conception, study design, execution, acquisition of data, analysis and interpretation, or in all these areas; took part in drafting, revising or critically reviewing the article; gave final approval of the version to be published; have agreed on the journal to which the article has been submitted; and agree to be accountable for all aspects of the work.

Disclosure

The authors report no conflicts of interest related to this work.

References

1. Chen Q, Thouas GA. Metallic implant biomaterials. *Mater Sci Eng R Rep*. 2015;87:1–57. doi:10.1016/j.mser.2014.10.001
2. Narushima T. 15 - New-generation metallic biomaterials. In: Niinomi M, editor. *Metals for Biomedical Devices*. Woodhead Publishing; 2010:355–378.
3. Williams DF. On the mechanisms of biocompatibility. *Biomaterials*. 2008;29(20):2941–2953. doi:10.1016/j.biomaterials.2008.04.023

4. Park J, Bauer S, Pittrof A, Killian MS, Schmuki P, von der Mark K. Synergistic control of mesenchymal stem cell differentiation by nanoscale surface geometry and immobilized growth factors on TiO2 nanotubes. *Small*. 2012;8(1):98–107. doi:10.1002/smll.201100 790

5. Park J, Bauer S, Schlegel KA, Neukam FW, von der Mark K, Schmuki P. TiO2 nanotube surfaces: 15 nm—an optimal length scale of surface topography for cell adhesion and differentiation. *Small*. 2009;5(6):666–671. doi:10.1002/smll.200801476

6. Minagar S, Wang J, Berndt CC, Ivanova EP, Wen C. Cell response of anodized nanotubes on titanium and titanium alloys. *J Biomed Mater Res A*. 2013;101A(9):2726–2739.

7. Zhang L-C, Chen L-Y A. Review on biomedical titanium alloys: recent progress and prospect. *J Biomed Mater Res A*. 2019;21 (4):1801215.

8. Liu X, Chu PK, Ding C. Surface modification of titanium, titanium alloys, and related materials for biomedical applications. *Mater Sci Eng R Rep*. 2004;47(3):49–121. doi:10.1016/j.mser.2004.11.001

9. Minagar S, Berndt CC, Wang J, Ivanova E, Wen C. A review of the application of anodization for the fabrication of nanotubes on metal implant surfaces. *Acta Biomater*. 2012;8(8):2875–2888. doi:10.1016/j.actbio.2012.04.005

10. Roy P, Berger S, Schmuki P. TiO2 nanotubes: synthesis and applications. *Angew Chem Int Ed*. 2011;50(13):2904–2939.

11. Kulkarni M, Mazare A, Gongadze E, et al. Titanium nanostructures for biomedical applications. *Nanotechnology*. 2015;26(6):062002. doi:10.1088/0957-4484/26/6/062002

12. Macak JM, Tsuchiya H, Ghicov A, et al. TiO2 nanotubes: self-organized electrochemical formation, properties and applications. *Curr Opin Solid State Mater Sci*. 2007;11(1):3–18. doi:10.1016/j.cossms.2007.08.004

13. Lee K, Mazare A, Schmuki P. One-dimensional titanium dioxide nanomaterials: nanotubes. *Chem Rev*. 2014;114(19):9385–9454. doi:10.1021/cr500061m

14. Bai Y, Park IS, Park HH, et al. The effect of annealing temperatures on surface properties, hydroxyapatite growth and cell behaviors of TiO2 nanotubes. *Surf Interface Anal*. 2011;43(6):998–1005. doi:10.1002/sia.3683

15. Huo K, Gao B, Fu J, Zhao L, Chu PK. Fabrication, modification, and biomedical applications of anodized TiO2 nanotube arrays. *RSC Adv*. 2014;4(33):17300–17324. doi:10.1039/C4RA01458H

16. Pérez DAG, Jorge Junior AM, Asato GH, et al. Surface anodization of the biphasic Ti13Nb13Zr biocompatible alloy: influence of phases on the formation of TiO2 nanostructures. *J Alloys Compd*. 2019;796:93–102. doi:10.1016/j.jallcom.2019.04.167

17. Pérez DAG, Jorge Junior AM, Roche V, et al. Severe plastic deformation and different surface treatments on the biocompatible Ti13Nb13Zr and Ti35Nb7Zr5Ta alloys: microstructural and phase evolutions, mechanical properties, and bioactivity analysis. *J Alloys Compd*. 2020;812:152116. doi:10.1016/j.jallcom.2019.152 116

18. Zhang H, Banfield JF. Phase transformation of nanocrystalline anatase-to-rutile via combined interface and surface nucleation. *J Mater Res*. 2000;15(2):437–448. doi:10.1557/JMR.2000.0067

19. Das K, Bose S, Bandyopadhyay A. TiO2 nanotubes on Ti: influence of nanoscale morphology on bone cell–materials interaction. *J Biomed Mater Res A*. 2009;90A(1):225–237.

20. Xiao X, Yu J, Tang H, Mao D, Wang C, Liu R. TiO2 nanotube arrays induced deposition of hydroxyapatite coating by hydrothermal treatment. *Mater Chem Phys*. 2013;138(2):695–702. doi:10.1016/j.matchemphys.2012.12.043

21. Hilario F, Roche V, Nogueira RP, Junior AMJ. Influence of morphology and crystalline structure of TiO2 nanotubes on their electrochemical properties and apatite-forming ability. *Electrochim Acta*. 2017;245:337–349.

22. Sista S, Wen C, Hodgson PD, Pande G. Expression of cell adhesion and differentiation related genes in MC3T3 osteoblasts plated on titanium alloys: role of surface properties. *Mater Sci Eng C*. 2013;33(3):1573–1582.

23. Liu L, Bhatia R, Webster TJ. Atomic layer deposition of nano-TiO(2) thin films with enhanced biocompatibility and antimicrobial activity for orthopedic implants. *Int J Nanomedicine*. 2017;12:8711–8723. doi:10.2147/IJN.S148065

24. Do Prado RF, Esteves GC, Santos ELS. In vitro and in vivo biological performance of porous Ti alloys prepared by powder metallurgy. *PLoS One*. 2018;13(5):e0196169. doi:10.1371/journal.pone.0196169

25. Roguska A, Pisarek M, Belcarz A, et al. Improvement of the biofunctional properties of TiO2 nanotubes. *Appl Surf Sci*. 2016; 388:775–785.

26. Beltrán-Partida E, Valdéz-Salas B, Moreno-Ulloa A, et al. Improved in vitro angiogenic behavior on anodized titanium dioxide nanotubes. *J Nanobiotechnology*. 2017;15(1):10. doi:10.1186/s12951-017-0247-8

27. Li Y, Gao Y, Shao B, Xiao J, Hu K, Kong L. Effects of hydrofluoric acid and anodised micro and micro/nano surface implants on early osseointegration in rats. *Br J Oral Maxillofac Surg*. 2012;50(8):779–783. doi:10.1016/j.bjoms.2011.12.008

28. Chen W-C, Ko C-L, Kuo H-N, et al. Mineralization of progenitor cells with different implant topographies. *Procedia Eng*. 2012;36:173–178. doi:10.1016/j.proeng.2012.03.027

29. Jie H, Zhou W, Zhou X, et al. The anatase phase of nanotopography titania plays an important role on osteoblast cell morphology and proliferation. *J Mater Sci Mater Med*. 2008;19(11):3465–3472. doi:10.1007/s10856-008-3505-3

30. Kokubo T, Takadama H. How useful is SBF in predicting in vivo bone bioactivity? *Biomaterials*. 2006;27(15):2907–2915. doi:10.1016/j.biomaterials.2006.01.017

31. Santana-Melo GF, Rodrigues BVM, da Silva E, et al. Electrospun ultrathin PBAT/nHAp fibers influenced the in vitro and in vivo osteogenesis and improved the mechanical properties of neoformed bone. *Colloids Surf B Biointerfaces*. 2017;155:544–552. doi:10.1016/j.colsurfb.2017.04.053

32. Mosmann T. Rapid colorimetric assay for cellular growth and survival: application to proliferation and cytotoxicity assays. *J Immunol Methods*. 1983;65(1):55–63. doi:10.1016/0022-1759(83)90303-4

33. Macak JM, Aldabergerova S, Ghicov A, Schmuki P. Smooth anodic TiO2 nanotubes: annealing and structure. *Phys Status Solidi A*. 2006;203(10):R67–R69. doi:10.1002/pssa.200622214

34. Zhao J, Wang X, Sun T, Li L. In situtemplated synthesis of anatase single-crystal nanotube arrays. *Nanotechnology*. 2005;16(10):2450–2454. doi:10.1088/0957-4484/16/10/077

35. Yang Y, Wang X, Li L. Crystallization and phase transition of titanium oxide nanotube arrays. *J Am Ceram Soc*. 2008;91(2):632–635. doi:10.1111/j.1551-2916.2007.02133.x

36. Varghese OK, Gong D, Paulose M, Grimes CA, Dickey EC. Crystallization and high-temperature structural stability of titanium oxide nanotube arrays. *J Mater Res*. 2003;18(1):156–165. doi:10.1557/JMR.2003.0022

37. Regonini D, Bowen CR, Jaroenworaluck A, Stevens R. A review of growth mechanism, structure and crystallinity of anodized TiO2 nanotubes. *Mater Sci Eng R Rep*. 2013;74(12):377–406.

38. Ghicov A, Macak JM, Tsuchiya H, et al. Ion implantation and annealing for an efficient N-doping of TiO2 nanotubes. *Nano Lett*. 2006;6(5):1080–1082. doi:10.1021/nl0600979

39. Malik H, Sarkar S, Mohanty S, Carlson K. Modelling and synthesis of magnéli phases in ordered titanium oxide nanotubes with preserved morphology. *Sci Rep*. 2020;10(1):8050. doi:10.1038/s41598-020-64918-0

40. Mazare A, Totea G, Burnei C, Schmuki P, Demetrescu I, Ionita D. Corrosion, antibacterial activity and haemocompatibility of TiO2 nanotubes as a function of their annealing temperature. *Corros Sci*. 2016;103:215–222.

41. Munirathinam B, Neelakantan L. Role of crystallinity on the nano-mechanical and electrochemical properties of TiO2 nanotubes. *J Electroanal Chem*. 2016;770:73–83.

42. Carnot A, Frateur I, Marcus P, Tribollet B. Corrosion mechanisms of steel concrete moulds in the presence of a demoulding agent. *J Appl Electrochem*. 2002;32(8):865–869. doi:10.1023/A:1020510506504

43. Chakri S, David P, Frateur I, et al. Effet de la composition chimique de la solution interstitielle de bétons jeunes sur la passivation d'un acier doux. *Mater Tech*. 2015;103(2):209.

44. Saji VS, Choe HC. Electrochemical corrosion behaviour of nanotubular Ti–13Nb–13Zr alloy in Ringer's solution. *Corros Sci*. 2009;51 (8):1658–1663. doi:10.1016/j.corsci.2009.04.013

45. Jianhua W, Toshio I, Naoto O, et al. Influence of surface wettability on competitive protein adsorption and initial attachment of osteoblasts. *Biomed Mater*. 2009;4(4):045002. doi:10.1088/1748-6041/4/4/045002

46. Eda DY, Robyn B, Daphne P, Fred A, Selçuk G, Wei S. Accelerated differentiation of osteoblast cells on polycaprolactone scaffolds driven by a combined effect of protein coating and plasma modification. *Biofabrication*. 2010;2(1):014109. doi:10.1088/1758-5082/2/1/014109

47. Khorasani MT, Mirzadeh H, Irani S. Plasma surface modification of poly (l-lactic acid) and poly (lactic-co-glycolic acid) films for improvement of nerve cells adhesion. *Radiat Phys Chem*. 2008;77 (3):280–287. doi:10.1016/j.radphyschem.2007.05.013

48. Law KY. Definitions for hydrophilicity, hydrophobicity, and super-hydrophobicity: getting the basics right. *J Phys Chem Lett*. 2014;5 (4):686–688. doi:10.1021/jz402762h

49. Anitha VC, Lee J-H, Lee J, Narayan Banerjee A, Woo Joo S, Ki Min B. Biofilm formation on a TiO2nanotube with controlled pore diameter and surface wettability. *Nanotechnology*. 2015;26(6):065102.

50. Liu G, Du K, Wang K. Surface wettability of TiO2 nanotube arrays prepared by electrochemical anodization. *Appl Surf Sci*. 2016;38 8:313–320.

51. Garlisi C, Trepci E, Li X, et al. Multilayer thin film structures for multifunctional glass: self-cleaning, antireflective and energy-saving properties. *Appl Energy*. 2020;264:114697. doi:10.1016/j.apenergy.2020.114697

52. Munirathinam B, Pydimukkala H, Ramaswamy N, Neelakantan L. Influence of crystallite size and surface morphology on electrochemical properties of annealed TiO2 nanotubes. *Appl Surf Sci*. 2015;355:1245–1253. doi:10.1016/j.apsusc.2015.08.017

53. Shokuhfar T, Hamlekhan A, Chang J-Y, Choi CK, Sukotjo C, Friedrich C. Biophysical evaluation of cells on nanotubular surfaces: the effects of atomic ordering and chemistry. *Int J Nanomedicine*. 2014;9:3737–3748. doi:10.2147/IJN.S67344

54. Kim M-J, Kim C-W, Lim Y-J, Heo S-J. Microrough titanium surface affects biologic response in MG63 osteoblast-like cells. *J Biomed Mater Res A*. 2006;79A(4):1023–1032. doi:10.1002/jbm.a.31040

55. Stein GS, Lian JB. Molecular mechanisms mediating proliferation/differentiation interrelationships during progressive development of the osteoblast phenotype. *Endocr Rev*. 1993;14(4):424–442. doi:10.1210/edrv-14-4-424

56. Wennerberg A, Jimbo R, Stübinger S, Obrecht M, Dard M, Berner S. Nanostructures and hydrophilicity influence osseointegration: a biomechanical study in the rabbit tibia. *Clin Oral Implants Res*. 2014;25 (9):1041–1050. doi:10.1111/clr.12213

57. Roman I, Trusca RD, Soare M-L, et al. Titanium dioxide nanotube films: preparation, characterization and electrochemical biosensitivity towards alkaline phosphatase. *Mater Sci Eng C*. 2014;37:374–382. doi:10.1016/j.msec.2014.01.036

58. Zuo J, Huang X, Zhong X, et al. A comparative study of the influence of three pure titanium plates with different micro- and nanotopographic surfaces on preosteoblast behaviors. *J Biomed Mater Res A*. 2013;101(11):3278–3284. doi:10.1002/jbm.a.34612

59. Li Y, Gao Y, Shao B, Xiao J, Hu K, Kong L. Effects of hydrofluoric acid and anodised micro and micro/nano surface implants on early osseointegration in rats. *J Oral Maxillofac Surg*. 2012;50(8):779–783.

60. Khrunyk YY, Belikov SV, Tsurkan MV, et al. Surface-dependent osteoblasts response to TiO2 nanotubes of different crystallinity. *Nanomaterials*. 2020;10(2):320. doi:10.3390/nano10020320

61. An SH, Narayanan R, Matsumoto T, Lee HJ, Kwon TY, Kim KH. Crystallinity of anodic TiO2 nanotubes and bioactivity. *J Nanosci Nanotechnol*. 2011;11(6):4910–4918. doi:10.1166/jnn.2011.4114